Separation Science and Technology
Publication details, including instructions for authors and subscription information:
http://www.informaworld.com/smpp/title~content=t713708471

Retention of Iron Oxide Particles by Stainless Steel and Magnetite Magnetic Matrix Elements in High-Gradient Magnetic Separation

Armin D. Ebner[a]; James A. Ritter[a]
[a] Department of Chemical Engineering, Swearingen Engineering Center, University of South Carolina, Columbia, South Carolina, USA

Online publication date: 08 July 2010

To cite this Article Ebner, Armin D. and Ritter, James A.(2004) 'Retention of Iron Oxide Particles by Stainless Steel and Magnetite Magnetic Matrix Elements in High-Gradient Magnetic Separation', Separation Science and Technology, 39: 12, 2863 — 2890
To link to this Article: DOI: 10.1081/SS-200028811
URL: http://dx.doi.org/10.1081/SS-200028811

SEPARATION SCIENCE AND TECHNOLOGY
Vol. 39, No. 12, pp. 2863–2890, 2004

Retention of Iron Oxide Particles by Stainless Steel and Magnetite Magnetic Matrix Elements in High-Gradient Magnetic Separation

Armin D. Ebner and James A. Ritter*

Department of Chemical Engineering, Swearingen Engineering Center, University of South Carolina, Columbia, South Carolina, USA

ABSTRACT

The retention performances of a novel 80 wt% magnetite-silica composite HGMS matrix element and a traditional stainless steel wool HGMS matrix element were compared. Breakthrough and ultimate (strictly magnetic) retention experiments were carried out at different feed concentrations, flow velocities, and magnetic field intensities with an aqueous slurry containing iron oxide (Fe_2O_3) particles. Results from the ultimate retention experiments were also compared to those obtained from a potential flow model. Overall, when supported by silica in the form of the 80 wt% magnetite-silica composite, magnetite was about 30 to 40% as effective as stainless steel in retaining iron oxide, which was quite

*Correspondence: James A. Ritter, Department of Chemical Engineering, Swearingen Engineering Center, University of South Carolina, Columbia, SC 29208, USA; Phone: (803) 777-3590; Fax: (803) 777-8265; E-mail: ritter@engr.sc.edu.

DOI: 10.1081/SS-200028811 0149-6395 (Print); 1520-5754 (Online)

encouraging when considering that the magnetic saturation of magnetite is about five times smaller than that of stainless steel. Magnetite is also less expensive than stainless steel wool, even when encased in silica gel, which makes its use as an HGMS matrix element even more attractive for certain applications. The ultimate retentions predicted from the model for both matrix elements were of the same order of magnitude as the experimental results, an encouraging result: under predictions no greater than a factor of 7 for the stainless steel cylinder, and over predictions no greater than a factor of 3 for the magnetite spheres were obtained. The reasons for these discrepancies centered on the relatively wide size distributions of the Fe_2O_3 particles and both the magnetic matrix elements, which were not accounted for by the models. The potential flow model also could not account for the effects of laminar layers and separation zones on retention; nor could it account for the effects of the changing flow patterns caused by particle build-up on retention. Also, the models could not predict the dependence of the ultimate retention on the feed concentration observed experimentally, which suggested the existence of dynamic equilibrium at the external boundaries of the collection zones where the magnetic force was weaker.

Key Words: Magnetic forces; High-gradient magnetic separation; Magnetic elements; Magnetite-silica composite; Iron oxide particles.

INTRODUCTION

The discovery of the significant role that magnetic field gradients play in enhancing the magnetic force over magnetic particles spawned a new type of magnetic separation process that exploits this principle to separate particles of small size and magnetic susceptibility. This new process, which has been coined high-gradient magnetic separation (HGMS) was first utilized in the early 1970s by the kaolin clay industry in the cleaning and brightening of china clay.[1–5] Since then HGMS has been utilized in many other applications, spanning from the removal of Fe and Ni particles from inks and toners[6] to the concentration and purification of radionuclides from nuclear facility effluents and high-level radioactive waste storage basins.[7–12]

The applications for HGMS technology have been extended even further by the use of magnetite (a highly magnetic form of iron oxide) as a metal ion adsorbent and flocculated seeding agent in the treatment of contaminated waters prior to its collection by HGMS.[13–20] An excellent example of this HGMS technology is the successful implementation of the SIROFLOC process.[21] A few years ago, however, in an altogether different approach,

Kochen and Navratil[22,23] and then Ebner et al.[24–26] demonstrated both experimentally and theoretically that magnetite could also be used as a stationary (fixed) matrix element in HGMS, a role that traditionally has been realized only by stainless steel. Despite having a magnetic saturation that is normally five times smaller than that of stainless steel, magnetite has some attributes that make it an attractive alternative to stainless steel for use as a matrix element in some HGMS processes.

First, magnetite is much less expensive and it is relatively easy to obtain in sizes below 1 μm. In contrast, wires made of stainless steel tend to be expensive, particularly if the diameter is smaller than 100 μm. The lack of a preferable orientation for magnetic retention due to the symmetry that is behind the relatively spherical shape of a magnetite particle is also an attractive advantage. This sphericity, ideally, causes the retention of magnetic particles to be the same on all magnetite particles. In contrast, however, no retention takes place on a stainless steel wire when the axis of the wire is parallel to the applied magnetic field, which causes approximately one-third of the wires in stainless steel wool to be magnetically inactive. The differences in the retention zones between spheres and cylinders relative to the orientation of the applied magnetic field are depicted in Fig. 1.

The much smaller diameter of magnetite (i.e., 0.2–1.0 μm) compared to the diameter of commonly used stainless steel wires (>50 μm) is without doubt the most attractive property that is fostering the use of magnetite as a matrix element in HGMS. Gradients and distortions of the magnetic field depend strongly on the curvature of the ferromagnetic matrix element and therefore increase inversely with the size of the matrix element. The effect of the smaller size of magnetite (despite its smaller saturation magnetization with respect to stainless steel) can be illustrated by comparing the magnetic force exerted over a particle by a spherical magnetite particle to that exerted by a stainless steel cylinder.[27] Eqs. (1) and (2) depict the magnetic force exerted on a particle of radius r_p, volume V_p and magnetic susceptibility χ_p:[27]

$$F_{s,r} = -2V_p(\chi_p - \chi_f)M_s \frac{R_s^3}{(R_s + R_p)^4}\left[H_o + \frac{2}{3}\left(\frac{R_s}{R_s + R_p}\right)^3 M_s\right] \quad (1)$$

$$F_{c,r} = -V_p(\chi_p - \chi_f)M_c \frac{R_c^2}{(R_c + R_p)^3}\left[H_o + \frac{1}{2}\left(\frac{R_c}{R_c + R_p}\right)^2 M_c\right] \quad (2)$$

at the point of strongest retention by a ferromagnetic sphere of radius r_s and cylinder of radius r_c, respectively, and at magnetic saturation. Using the saturation magnetization values of magnetite (M_s) and stainless steel (M_c) provided in Table 1, the smallest suspended particle that is removable by a

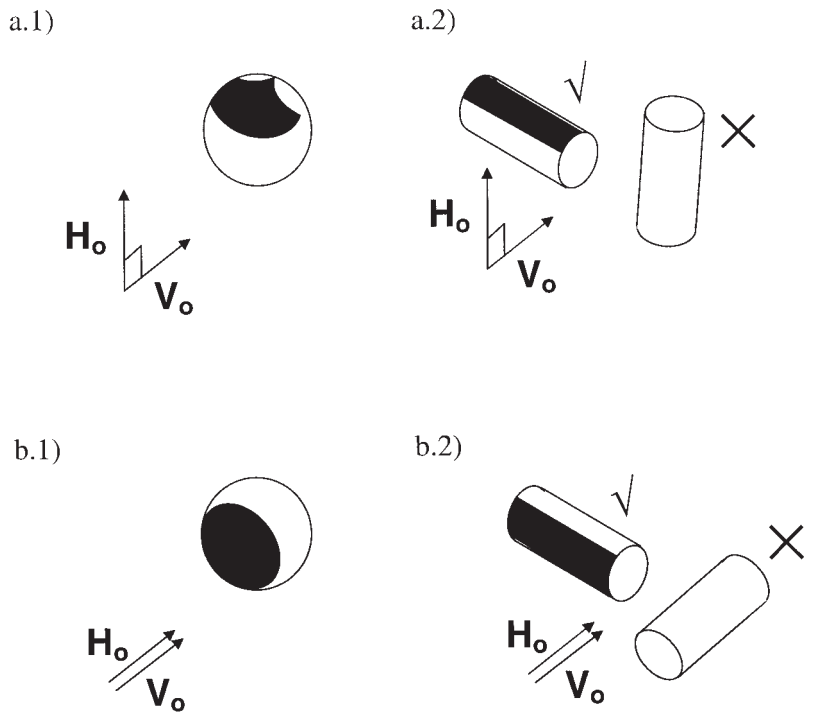

Figure 1. Collection zones (in black) on a ferromagnetic 1) sphere and 2) cylinder when magnetic and flow fields are a) perpendicular and b) parallel to each other. In the case of the cylinder, the checks and crosses indicate maximum and no retention obtained when the axis of the cylinder is perpendicular and parallel to the magnetic field, respectively.

spherical magnetite particle of 1 μm diameter and a cylindrical stainless steel wire of 50 μm diameter, for a range of magnetic susceptibilities ($\chi_f = 0$) under two different applied magnetic fields (0.3 and 3.0 T) is presented in Fig. 2. The minimum size of the retained particle for each case was obtained by evaluating the radius R_p for which the relationship:[24]

$$F_{M,c \text{ or } s,r} = \frac{10k_bT}{R_p} \tag{3}$$

is satisfied, where k_b is the Boltzmann constant and T is the absolute temperature. Eq. (3) indicates that the condition for particle retention is when the magnetic force on the particle is at least 10 times larger than the Brownian force exerted upon it.

Table 1. Values of the parameters utilized in the theoretical model.

H_o	$6.37 \times 10^5\ \mathrm{A\,m^{-1}}$
$M_{s,s}$[a]	$4.85 \times 10^5\ \mathrm{A\,m^{-1}}$
$M_{s,c}$[a]	$1.65 \times 10^6\ \mathrm{A\,m^{-1}}$
η_w	$1.00 \times 10^{-3}\ \mathrm{Kg\,s^{-1}\,m^{-1}}$
χ_p[b]	3.59×10^{-3}
ρ_c	$7.80\ \mathrm{g\,cm^{-3}}$
ρ_s	$5.18\ \mathrm{g\,cm^{-3}}$
ρ_p	$5.24\ \mathrm{g\,cm^{-3}}$
R_c	50.00 μm
R_s[c]	2.12 μm
R_p[c]	4.67 μm
$R_{m\text{-}s}$	187.50 μm

[a]Obtained with a Quantum Design MPMS XL SQUID at 25°C.
[b]Reference[46].
[c]Obtained from log-normal fits of the experimental data obtained from an Accusizer Optical Particle Sizer, Model 770A.

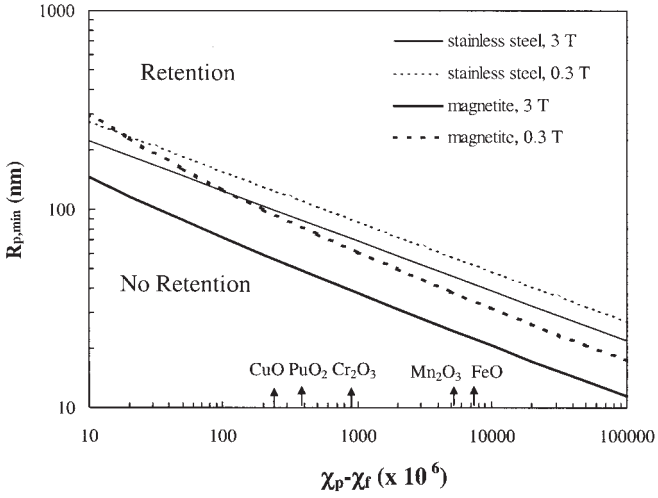

Figure 2. Relationship between smallest particle retainable and the relative magnetic susceptibility for a 1-μm-diameter spherical magnetite particle and a 50-μm-diameter stainless steel wire at two different magnetic field intensities of 0.3 and 3.0 T.[27] The relative magnetic susceptibility of various paramagnetic metal oxides is also shown.

The results in Fig. 2 clearly confirm that a 1 μm diameter magnetite sphere is a more effective HGMS ferromagnetic element than a 50 μm diameter stainless steel wire when retaining smaller particles. In fact, within the range of magnetic susceptibilities for typical paramagnetic oxides (also shown in Fig. 2), the magnetite sphere outperforms the stainless steel wire even when the magnetic field intensity is 10 times smaller. Nevertheless, due to its small size, magnetite cannot be used alone in an HGMS column without first being supported by a material of much larger size; otherwise, appreciable pressure drops can occur along the bed. Kochen and coworkers[22,23] solved this problem by coating spherical particles (0.063 to 0.125 mm diameter) with a polyamine epichlorohydrin resin. Alternatively, Shen et al.[28] showed that it is possible to make a large composite particle composed of small magnetite particles (clusters) encased in a silica gel matrix, containing up to 80 wt% magnetite.

The objective of this study is to compare the performance of the 80 wt% magnetite-silica composite HGMS matrix element with a commercially available stainless steel wool HGMS matrix element in retaining iron oxide (Fe_2O_3) particles. Breakthrough experiments, as well as ultimate retention experiments (as explained later), were carried out using different feed concentrations, flow velocities, and magnetic fields. Also, the ultimate retention experimental results were contrasted against a theoretical model that was developed to corroborate the experimental findings.

EXPERIMENTAL

The permanent magnet assembly obtained from MagnetSales & Manufacturing, Inc. is shown in Fig. 3a and was used to carry out all of the experiments. It consisted of two pieces of NdFeB with dimensions of $2 \times 3 \times 4$ cm and with the 3×4 cm sides facing each other. Each piece was soldered to the jaw of a vise to easily adjust the magnetic field by separating the two pieces of magnet from each other. Under all magnet separations, the magnetic field was relatively constant in the gap between the magnetic pieces where the column was located. Figure 3b depicts the experimental setup utilized to carry out both the breakthrough and ultimate retention experiments. Suspensions of Fe_2O_3 (Aldrich, 99%) were prepared in a mechanically stirred 5 gal tank. Using a peristaltic pump, the Fe_2O_3 suspension was pumped through a 1-cm-diameter (ID) glass column (chromatoflex, Kontex) placed within the gap of the permanent magnet assembly. Either 4.0 grams of the 80 wt% magnetite-silica composite or 1.0 g of stainless wool was placed inside the column to serve as the HGMS matrix element. The size of the magnetite-silica composite particles corresponded to 35–60 Tyler mesh size (i.e., $\bar{r}_{s-m} = 187.5$ μm). The number of particle size distributions of both the Fe_2O_3 particles in the

a)

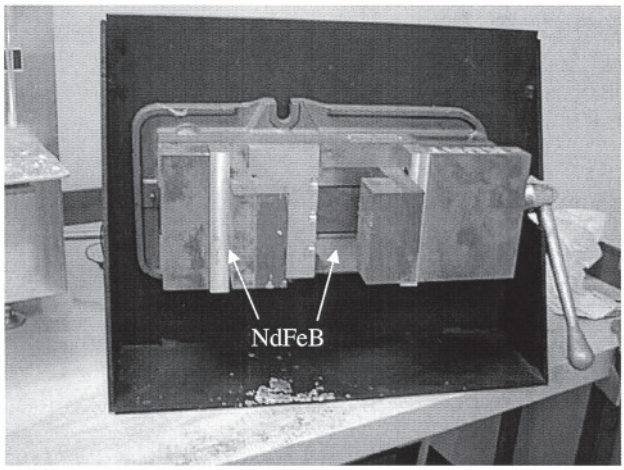

b)

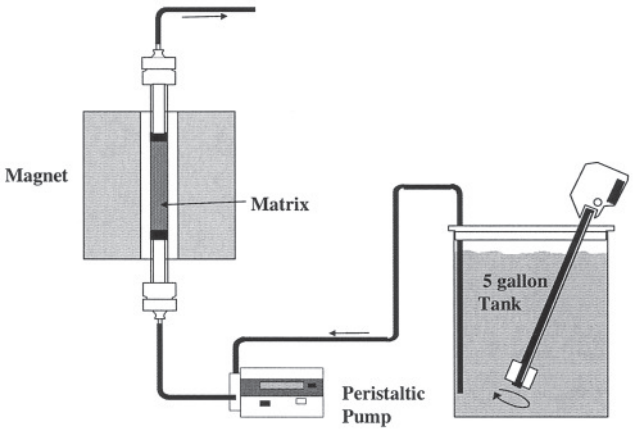

Figure 3. a) Photograph of the 0.8 T NdFeB permanent magnet assembly, and b) schematic of the experimental breakthrough and ultimate retention flow apparatus. The two pieces of NdFeB permanent magnet inside the assembly are indicated by the arrows in a).

suspensions and the magnetite particles when suspended in an aqueous solution where obtained with an optical particle sizer, Accusizer Model 770A.

For the breakthrough experiments, the feed concentration of Fe_2O_3 was kept constant at 0.5 g/L, and the feed velocity was maintained at 1.06 cm s^{-1}. The magnetic field strength at the location of the matrix was also held constant during each breakthrough experiment. Different magnetic field strengths of 0.0, 0.254, 0.4, and 0.8 T were investigated by changing the gap between the two magnetic pieces. The strength of the magnetic field was measured using a gauss meter (Model 4048, F. W. Bell). The breakthrough of suspended Fe_2O_3 particles was monitored by the continuous collection of the effluent in 30 mL plastic bottles until about 5 L of solution was fed into the column. The concentration of the Fe_2O_3 particles in the collected samples was determined gravimetrically by first determining the weight of solution collected in the bottles. This was realized by weighing the bottles prior to and after filling them up with collected solution. The concentration of Fe_2O_3 particles was then calculated using the corresponding weight of collected solution in the sample and by measuring the amount of Fe_2O_3 solids contained in it through membrane filtration (Gelman Sciences 0.45-μm Tuffryn®) and vacuum drying at 80°C overnight. Breakthrough experiments were carried out in this manner using both types of HGMS matrix elements.

The ultimate retention experiments were carried out at a constant magnetic field strength of 0.8 T, Fe_2O_3 feed concentrations between 0.5 to 3.0 g/L, and feed velocities between 1.06 and 3.18 cm s^{-1}. Again, both types of matrix elements were used. With the column placed in between the magnet assembly gap, the matrix was fed until it became saturated. Based on the results obtained from the breakthrough experiments, about 2 h was deemed sufficient to saturate the matrix elements with retained Fe_2O_3 particles. Then the feed was replaced with clean water flowing at the same rate for an additional 2 h while still under the influence of the magnetic field, flushing the Fe_2O_3 particles from the void spaces in the column and removed any loosely (physically) retained Fe_2O_3 particles. Finally, with the clean water still flowing through the column, the magnet assembly was removed causing the spontaneous release of the Fe_2O_3 particles retained only magnetically by the matrix. This effluent was collected in 2 L bottles. The total amount of magnetically retained solids (termed here as the ultimate retention) was calculated using the same procedure as in the breakthrough experiments.

THEORETICAL

It must be emphasized at the outset that the estimation of the maximum solids holdup by magnetic wires or spheres is often complex and seldom

accurate, due to the highly dynamic nature of the process involved. Basically, magnetic elements always experience changes of the flow patterns around the capture zone due to the continuous capture and build-up of new material until saturation. The main difficulty is that there are no simple analytical models that accurately predict these ever-changing flow patterns around the magnetic element. Consequently, most current investigators have been forced to rely on analytical expressions that describe the flow patterns around spheres and cylinders at the early stages of loading. The two approaches normally used are strictly limited to the low Reynolds regime, i.e., a laminar flow model ($N_{RE} < 1$),[29–32] or to potential flow conditions,[33–36] where it is assumed that laminar layers do not exist (i.e., high Reynolds numbers) and separation zones are absent (in reality, these two conditions are never met simultaneously). The latter approach is adopted here, because it is considered to be more representative of the conditions used in the ultimate retention experiments.

Models describing static force balances between the magnetic force and the drag force over a suspended particle under potential flow are developed for the two geometries considered here (i.e., the cylinder and the sphere). Due to the orientation of the magnetic field associated with the permanent magnet assembly, both types of matrix elements (i.e., stainless wool and magnetite-silica composite) are assumed to be under the transverse configuration, i.e., the flow and magnetic fields are assumed to be perpendicular to each other. Figure 4 shows the approximate collection zones for a cylinder (Fig. 4a) and a sphere (Fig. 4b) under this situation. The LHS shows 3-D schematics depicting the collection zones for each case, while the RHS shows a profile of the collection zones (in gray) for the 2-D cross-sectional plane depicted in the 3-D schematics. Besides being parallel to the magnetic field, in the case of the cylinder (Fig. 4a), the 2-D cross sectional plane is also perpendicular to the cylinder axis. In the case of the sphere (Fig. 4b), however, the 2-D cross-sectional plane (plane A in Fig. 4b) also contains the center of the sphere rotated an angle ϕ around the z-axis with respect to the plane containing the fluid velocity at infinity (plane z-y in Fig. 4b).

In the case of the cylinder, identical profiles of the collection zone are obtained for any cross-sectional plane that is parallel to the one presented in Figure 4a. Therefore, the total mass of solids collected per mass of wire only requires the determination of the gray area depicted in the RHS of Fig. 4a, i.e.,

$$q_c = f_c(1 - \varepsilon_p)\frac{\rho_p}{\rho_c}\frac{2}{\pi R_c^2}\int_0^{\pi}(r_{ext}^2 - r_{int}^2)d\theta \tag{4}$$

where r_{ext} and r_{int} are the distances of the external and internal boundaries from the center of the cylinder in polar coordinates, f_c is an efficiency factor that equals two-thirds and accounts for the fact that about two-thirds of the wires

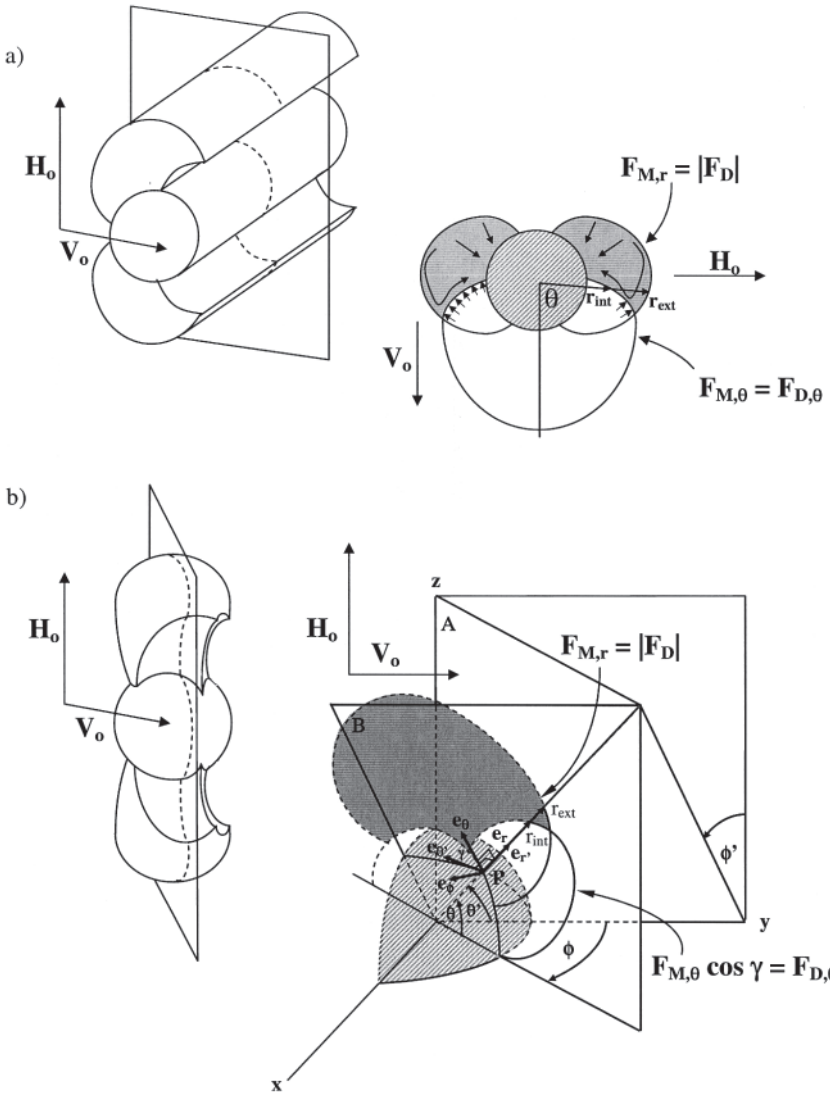

Figure 4. Schematics depicting the determination of the collection zones in a ferromagnetic a) cylinder and b) sphere. Schematics on the RHS indicate the 2-D collection profiles (zones in gray) for the cross-sectional plane depicted in the 3-D schematics on the left. In the case of the cylinder, the cross-sectional planes are all parallel to each other and perpendicular to the axis of the cylinder. In the case of the sphere, the cross-sectional planes bisect the ferromagnetic sphere, as indicated by plane A in the schematic on the RHS; the schematic on the RHS also shows that the velocity vector is located at point P in plane B.

are effectively oriented for retention, and $\varepsilon_{Fe_2O_3}$ is the porosity of the retained Fe_2O_3. The boundaries of the gray zones in Fig. 4a are defined by the following relationships:

$$F_{M,c,r} = |\mathbf{F_{D,c}}| \tag{5}$$

$$F_{M,c,\theta} + F_{D,c,\theta} = 0 \tag{6}$$

where $F_{M,c}$ and $\mathbf{F_{D,c}}$ are respectively the magnetic and drag forces on the suspended particle, and the subscripts r and θ stand for the components of these forces in polar coordinates, and subscript c stands for cylinder. The solution of the equations for a given angle θ are, respectively, r_{ext} and r_{int}, with their minimum values being the radius of the wire. It must be noted that the condition in Eq. (5) has been utilized instead of $F_{M,c,r} = F_{D,c,r}$, due to the fact that under the potential flow assumption and transverse configuration the solution of the latter relationship is found only at infinity where the total loading is impossible to determine. It is also noteworthy that the intersection zone of the regions defined by the solutions of Eqs. (5) and (6) does not retain particles. Despite the fact that within this region the radial component of the force over the particle is inward (i.e., attractive), particles that reach the upper boundary (as shown in Fig. 4a) are impeded from going any further inward due to the opposing tangential component $F_{M,c,\theta}$ of the magnetic force.

The expressions, in dimensionless form, that define the components of the magnetic force on a spherical particle of magnetic susceptibility χ_p and radius r_p by a cylindrical ferromagnetic wire of saturation magnetization $M_{s,c}$ and radius r_c when the applied magnetic field is H_o are given by:[20,31–43]

$$F_{M,c,r} = -\frac{V_{m,c}}{V_o}\left(\frac{R_c}{r}\right)^3\left[-\cos 2\theta + k_c\left(\frac{R_c}{r}\right)^2\right] \tag{7a}$$

$$F_{M,c,\theta} = \frac{V_{m,c}}{V_o}\left(\frac{R_c}{r}\right)^3 \sin 2\theta \tag{7b}$$

where $V_{m,c}$ is the so called magnetic velocity given by

$$V_{m,c} = \frac{4}{9}\frac{R_p^2}{R_c}\mu_o\frac{\chi_p - \chi_f}{\eta_f}k_c H_o^2 \tag{8}$$

and k_c is the demagnetizing factor of the cylinder. Because the stainless steel is ferromagnetically soft, k_c is related to the applied magnetic field H_0 through:[27,31,37,38]

$$k_c = Min\left(1, \frac{M_{sat,c}}{2H_o}\right) \tag{9}$$

where $M_{sat,c}$ is the magnetization of the cylinder at saturation. The dimensionless components of the drag force about the cylinder are given by

$$F_{D,c,r} = \left[1 - \left(\frac{R_c}{r}\right)^2\right] \cos\theta \tag{10a}$$

$$F_{D,c,\theta} = -\left[1 + \left(\frac{R_c}{r}\right)^2\right] \sin\theta \tag{10b}$$

In the case of the spherical magnetite-silica composite matrix element, the profiles of the collection zone determined by the 2-D cross-sectional plane vary according to the angle ϕ that this plane makes with the z-y plane (as shown in Fig. 4b.) The total mass of solids collected per mass of magnetite is thus given by:

$$q_s = f_s(1 - \varepsilon_p)\frac{\rho_p}{\rho_s}\frac{1}{\pi R_s^3}\int_{\phi=0}^{\pi}\int_{\theta=0}^{\pi/2}(r_{ext}^3 - r_{int}^3)\sin\theta d\theta d\phi \tag{11}$$

where as before, r_{ext} and r_{int} represent the distances of the external and internal boundaries from the center of the sphere. Here, the efficiency factor f_s accounts for the fact that magnetic retention takes place only on those magnetite particles that are exposed at the surface of the composite particles. By assuming only half of the volume of these magnetite particles is exposed at the surface of a magnetite-silica composite particle for magnetic retention, it is relatively easy to prove that:

$$f_s = 2\frac{R_s}{R_{m\text{-}s}} \tag{12}$$

where R_{m-s} is the radius of the magnetite-silica composite particle and R_s is the radius of the magnetite particle (typically comprised of a cluster of magnetite crystals).

Special geometrical considerations must be accounted for when determining the boundaries of the collection zone around the spherical magnetite particle (cluster). First, it must be realized that all the velocities of the fluid around the sphere are contained in planes that both bisect the sphere and are parallel to the y-axis (i.e., parallel to the velocity of the flow at infinity $\mathbf{V_o}$). Consequently, for any point in space, the corresponding direction of the drag force does not necessarily rest in the same plane associated with the direction of the magnetic force, which is the 2-D cross-sectional plane A mentioned earlier. For point P shown in Fig. 4b, for example, the plane containing the flow velocity, labeled as B, is inclined at angle ϕ' with respect to the z-y plane around the y-axis. As a result, it is convenient to choose two

systems of spherical coordinates, namely, one with parameters r, θ, and ϕ that define the planes containing the direction of the magnetic force simply by the angle ϕ (such as A, for example) and one with parameters r′, θ', and ϕ' that define the planes containing the direction of the drag force simply by the angle ϕ' (such as B, for example). Both systems of coordinates still have their origin at the center of the magnetite sphere; and since the planes containing P (namely A and B) bisect the magnetite sphere, the line of intersection of these planes passes through both point P and the center of the sphere. Hence, these coordinate systems also share the same radial directional vector ($\mathbf{e_r} = \mathbf{e_{r'}}$) as Fig. 4b depicts. This in turn forces the directional vector $\mathbf{e}_{\theta'}$ of the second system of coordinates to lie in the same plane defined by the directional vectors $\mathbf{e}_\theta$ and $\mathbf{e}_\phi$ of the first coordinate system.

By defining γ as the angle between $\mathbf{e}_\theta$ and $\mathbf{e}_{\theta'}$, the components of the drag force in the system of coordinates r, θ, ϕ become:

$$F_{D,s,r} = F_{D,s,r'} \tag{13a}$$

$$F_{D,s,\theta} = F_{D,s,\theta'} \cos\gamma \tag{13b}$$

$$F_{D,s,\phi} = F_{D,s,\theta'} \sin\gamma \tag{13c}$$

where $F_{D,r'}$ and $F_{D,\theta'}$ are given by:

$$F_{D,s,r'} = \left[1 - \left(\frac{R_s}{r}\right)^3\right] \cos\theta' \tag{14a}$$

$$F_{D,s,\theta'} = -\left[1 + \frac{1}{2}\left(\frac{R_s}{r}\right)^3\right] \sin\theta' \tag{14b}$$

Using the following trigonometric relationships that naturally arise from the existing spatial relationships between the two coordinate systems:

$$\cos\theta' = \cos\theta\cos\phi \tag{15}$$

$$\sin\theta'\cos\phi' = \sin\theta \tag{16}$$

$$\sin\theta'\sin\phi' = \cos\theta\sin\phi \tag{17}$$

$$\cos\theta'\sin\phi' = \sin\gamma\cos\phi - \cos\gamma\sin\theta\sin\phi \tag{18}$$

$$\sin\theta' = \sin\gamma\sin\phi + \cos\gamma\sin\theta\cos\phi \tag{19}$$

$$\cos\theta'\cos\phi' = \cos\gamma\cos\theta \tag{20}$$

the following expressions for the components of the drag force in Eqs. (13a), (13b), and (13c) result:

$$F_{D,s,r} = \left[1 - \left(\frac{R_s}{r}\right)^3\right] \cos\theta \cos\phi \tag{21a}$$

$$F_{D,s,\theta} = -\left[1 + \frac{1}{2}\left(\frac{R_s}{r}\right)^3\right] \sin\theta \cos\phi \tag{21b}$$

$$F_{D,s,\phi} = -\left[1 + \frac{1}{2}\left(\frac{R_s}{r}\right)^3\right] \sin\phi \tag{21c}$$

Based on the same arguments utilized to determine the collection zones in the cylindrical case, the radial component of the magnetic force is equated to

$$F_{M,s,r} = |\mathbf{F_{D,s}}| \tag{22}$$

However, due to the fact that the tangential component of the magnetic force is inclined at angle γ with respect to the tangential component of the drag force, the following relationship is used instead:

$$F_{M,s,\theta} \cos\gamma + F_{D,s,\theta'} = 0 \tag{23}$$

which after using Eqs. (15) through (20) is given by:

$$F_{M,s,\theta} = \left[1 + \frac{1}{2}\left(\frac{R_s}{r}\right)^3\right] \frac{1 - \cos^2\theta \cos^2\phi}{\cos\phi \sin\theta} \tag{24}$$

The components of the magnetic force corresponding to the magnetite sphere of radius R_s are given by:[24–27,33,34]

$$F_{M,s,r} = -\frac{V_{m,s}}{V_o}\left(\frac{R_s}{r}\right)^4 \left[\frac{1 - 3\cos 2\theta}{2} + \frac{5 - 3\cos 2\theta}{2} k_s \left(\frac{R_s}{r}\right)^3\right] \tag{25a}$$

$$F_{M,s,\theta} = \frac{V_{m,s}}{V_o}\left(\frac{R_s}{r}\right)^4 \left[1 + \frac{k_s}{2}\left(\frac{R_s}{r}\right)^3\right] \sin 2\theta \tag{25b}$$

where $M_{sat,s}$ is the magnetic saturation of magnetite. The corresponding relationships for the magnetic velocity $V_{m,s}$ and the demagnetizing factor k_s for a soft ferromagnetic sphere are given by:[27]

$$V_{m,s} = \frac{2}{3}\frac{R_p^2}{R_s}\mu_o \frac{\chi_p - \chi_f}{\eta_f} k_s H_o^2 \tag{26}$$

$$k_s = Min\left(1,\ \frac{M_{sat,s}}{3H_o}\right) \tag{27}$$

The following methodology was developed to theoretically predict the ultimate retention of Fe_2O_3 particles by the cylindrical stainless steel and spherical magnetite-silica composite matrix elements. For each case, the properties of the medium, i.e., χ_f and η_f, and those of the Fe_2O_3 particles, i.e., R_p, χ_p, ρ_p and ε_p, were known. In the case of the cylindrical stainless steel wire, the following additional properties were known: R_c, $M_{sat,c}$, and ρ_c; and similarly, in the case of the spherical magnetite-silica composite, the following additional properties were known: R_s, $R_{m\text{-}s}$, $M_{sat,s}$, and ρ_s. For the cylindrical stainless steel wire, r_{ext} and r_{int} were obtained from Eqs. (5) and (6) for varying values of θ ($0 \le \theta \le \pi$) and a given value of the applied magnetic field H_o by solving Eqs. (5) and (6) together with Eqs. (7) through (10), which added a total of six additional equations that accounted for the following six unknowns: $F_{M,c,r}$, $F_{M,c,\theta}$, $V_{m,c}$, k_c, $F_{D,c,r}$, and $F_{D,c,\theta}$. For the spherical magnetite-silica composite, r_{ext} and r_{int} were obtained from Eqs. (22) and (24) for varying values of θ ($0 \le \theta \le \pi/2$) and ϕ ($0 \le \phi \le \pi$) and a given value of the applied magnetic field H_o by solving Eqs. (22) and (24) together with Eqs. (21), (25), (26), and (27), which added a total of seven additional equations that accounted for the following seven unknowns: $F_{M,s,r}$, $F_{M,s,\theta}$, $V_{m,s}$, k_s, $F_{D,s,r}$, $F_{D,s,\theta}$, and $F_{D,s,\phi}$. With r_{ext} and r_{int} determined for each case, Eqs. (4) and (11) were used to calculate the total mass of solids collected per mass of matrix element in the cylindrical wire and the spherical magnetite-silica composite particles, respectively.

RESULTS AND DISCUSSION

The breakthrough results obtained with each of the matrix elements, i.e., with the 80 wt% magnetite-silica composite and the stainless steel wool, are shown in Fig. 5. Four different magnetic field strengths of 0.0, 0.254, 0.40, and 0.8 T were investigated, with the superficial velocity fixed at 1.06 cm/s (which corresponds to a flow rate of 50 mL/min) in all runs. Figure 5a depicts the concentration of the suspended ferric oxide particles in the effluent during the first hour of breakthrough while feeding 0.5 g/L solution of Fe_2O_3

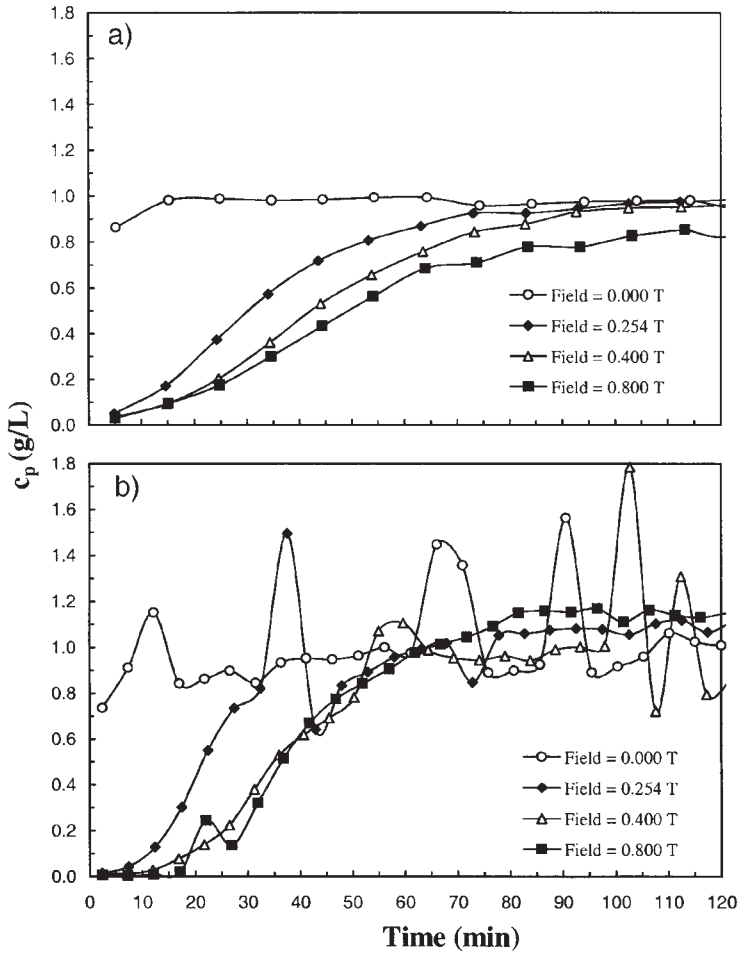

Figure 5. Experimental breakthrough curves showing the effect of the magnetic field intensity ($\mu_o H_o = 0.0$, 0.254, 0.400 and 0.800 T) on retention of Fe_2O_3 particles by a) 4.0 g of the 80 wt% magnetite-silica composite, and b) 1.0 g of the stainless steel wool for a fixed superficial velocity (U_o) of 1.06 cm s^{-1} and suspended solids feed concentration of 0.5 g L^{-1}.

through 4.0 g of the magnetite-silica composite matrix element; similarly, Fig. 5b depicts the results obtained while feeding 0.5 g/L solution of Fe_2O_3 through 1.0 g of the stainless steel wool matrix element. First and foremost notice that for both matrix elements, when no magnetic field was applied, breakthrough occurred immediately; in contrast, when the magnetic field

was applied both matrix elements exhibited significant delay in breakthrough, indicating magnetic retention. An interesting feature of the breakthrough profiles obtained with the magnetite-silica composite compared to those obtained with the stainless steel wool was their much smoother appearance. This result suggested, perhaps, the ability of the magnetite-silica composite to stabilize the interstitial flow and hence minimize release after capture. However, breakthrough for the magnetite-silica composite matrix occurred sooner and the profiles were broader than those obtained with the stainless steel wool matrix; nevertheless, the marked magnetic effect exhibited by the magnetite-silica composite was quite obvious and substantial, which validates the use of this material as an HGMS matrix element. About 3.2 g of magnetite (i.e., 80% of 4 g) exhibited a magnetic behavior that was comparable to 1.0 g of stainless steel wool, which according to Eq. (12) and the data given in Table 1, was the result of approximately 2% (i.e., $f_s = 0.0022$) of the magnetite being available at the surface of the composite particles for retention. Whether this significant result was due to the synergistic effect of the magnetite-silica composite particles operating as one large particle[44,45] or the individual magnetite particles is not known at this time and requires further verification.

A comparison between the two matrix elements can be quantified by analyzing the following integral expressions that describe the mass balances about the breakthrough curves:

$$q_{c,BT} = \frac{c_o \dot{V}}{m_c} \int_0^t \left(1 - \frac{c}{c_o}\right) dt \tag{28a}$$

$$q_{s,BT} = \frac{c_o \dot{V}}{m_s} \int_0^t \left(1 - \frac{c}{c_o}\right) dt \tag{28b}$$

where $q_{c,BT}$ and $q_{s,BT}$ are the grams of Fe_2O_3 retained in the column (both liquid and retained phases) per gram of matrix element, c_o is the feed concentration, and V is the feed flow rate. The results are presented in Table 2. They indicate that the performance of magnetite as a matrix element was about 30 to 40% as effective as stainless steel wool. Very similar performance differences were obtained from 21 ultimate retention experiments, the results of which are presented in Table 3. Depending on the feed velocity and flow rate, the ultimate retention of Fe_2O_3 by the magnetite-silica composite matrix element varied between 0.42 to 0.67 g/g, whereas the range for the stainless steel matrix element varied between 1.13 and 1.85 g/g, about two to three times greater. Comparing the values in Tables 2 and 3 also shows that the retention during breakthrough was essentially caused by magnetic retention and not physical filtration. In general, the ultimate retention was independent of the

Table 2. Experimental loading of Fe_2O_3 particles obtained by integrating the breakthrough curves shown in Fig. 5 according to Eqs. (28a) and (28b), respectively, for stainless steel wool ($q_{c,BT}$) and 80 wt% magnetite-silica composite ($q_{s,BT}$) matrix elements: $U_o = 1.06\,cm/s$, $C_o = 0.5\,g/L$, $m_c = 1.0\,g$ and $m_s = 4.0\,g$.

$\mu_o H_o$ (T)	$q_{c,BT}$ (g/g)	$q_{s,BT}$ (g/g)[a]
0.000	~0.0	~0.0
0.254	0.439	0.228
0.400	0.869	0.312
0.800	1.318	0.456

[a]Values based on pure magnetite, i.e., 3.2 g.

Table 3. Experimental and theoretical (model) ultimate retentions of Fe_2O_3 particles (g/g) by stainless steel wool and 80 wt% magnetite-silica composite matrix elements for a magnetic field strength ($\mu_o H_o$) of 0.8 T, and different feed concentrations (c_o) and superficial velocities (U_o).

	U_o (cm/s)		
c_o (g/L)	1.06	2.12	3.18
Stainless steel wool matrix element			
0.5	1.35	1.13	—
1.0	1.36	1.23	1.32
2.0	1.65	1.36	1.46
3.0	1.85	1.56	1.47
Model	0.39	0.27	0.22
	1.06	1.59	2.12
80 wt% Magnetite-silica composite matrix element			
0.5	0.46	0.60	—
1.0	0.49	0.42	0.42
2.0	0.55	—	0.56
3.0	0.60	0.67	0.45
Model[a]	1.76	1.30	1.05

[a]Values based on pure magnetite, i.e., 3.2 g.

feed velocity and increased slightly with the feed concentration. These last trends are treated below in context to the predictions of the ultimate retentions from the model, which are also shown in Table 3. The parameters utilized in the model are presented in Table 1.

Because of the inherent difficulty of mathematically describing the flow behavior around these kinds of HGMS matrix elements, it was somewhat surprising yet encouraging that the predictions of the ultimate retentions from the models were of the same order of magnitude as the experimental results. In the case of the stainless steel cylinder, the model under-predicted the experimental results by as much as a factor of 7, whereas in the case of the magnetite spheres, the model over-predicted the experimental results but only by as much as a factor of 3. Several reasons for these discrepancies are offered. First, as discussed previously, although mathematically attractive, the potential flow assumption hardly represents the behavior of the flow around an actual matrix element due to the fact that it does not account for laminar layers and separation zones, and more importantly, it assumes that the flow pattern around the matrix element does not change with the Fe_2O_3 loading. In the case of the stainless steel wire, for example, the existence of laminar zones around the wires, that would necessarily allow for more retention, could explain the under-prediction of the experimental results. A different explanation was needed for the magnetite-silica composite, since the model over-predicted the experimental results. In this case it was surmized that the model over-predicted the ultimate retention because it utilized a magnetite particle that had a radius of 2.12 μm, where in reality the effective particle size was probably much smaller with radii on the order of 250 nm (see below). A much smaller magnetite particle (cluster) would not have been able to attract and retain the rather large Fe_2O_3 particles with radii of 4.67 μm.[44] It was further surmized that this effect must have overwhelmed the opposite effect associated with the fact that the model for the magnetite-silica composite did not consider the large laminar layers that surrounded the magnetite-silica composite particles, which would necessarily have allowed for more retention than that predicted by the model, just as in the case of the stainless steel wire matrix.

Another element of uncertainty imparted to the models was the assumption of size uniformity of the ferromagnetic matrix elements and the paramagnetic Fe_2O_3 and magnetite particles. Figure 6 shows several scanning electron micrographs (SEM) of the stainless steel matrix element wires to illustrate this point. In general, the wires exhibited radii distributions ranging between 10 and 80 μm. The irregularity also extended to the individual wires themselves. Observe, for example, that the tip at the bottom part of the wire in Fig. 6b was about 25 μm thick, whereas the main body of the wire was several times larger, with thicknesses varying between

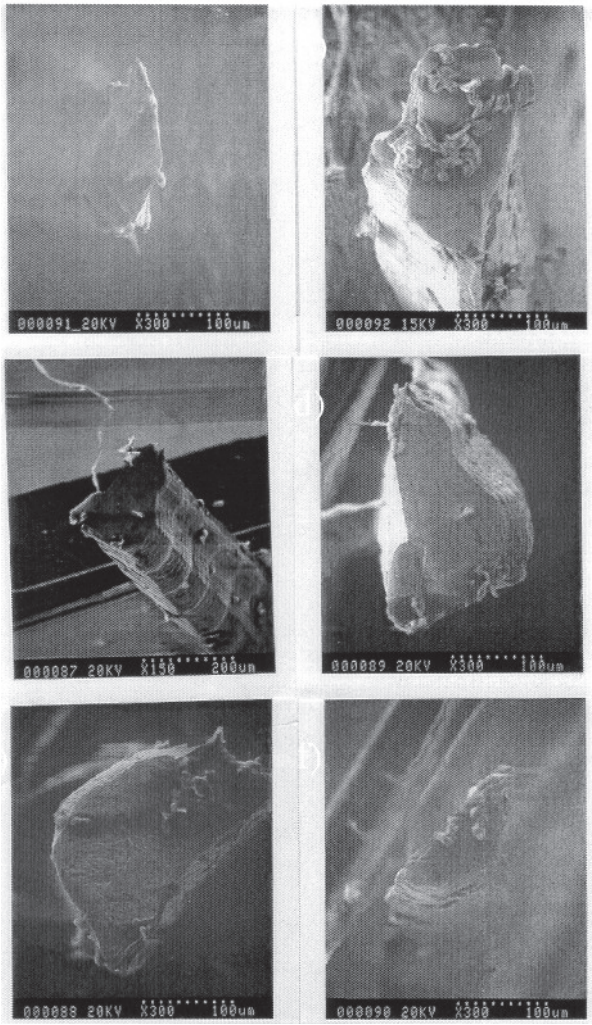

Figure 6. Scanning electron micrographs (SEMs) of the stainless steel wire matrix element, revealing the variability of the wires used in the HGMS unit.

80 and 130 μm. Due to the model requiring only a single value for r_c, a wire radius of 50 μm was assumed. The under-prediction of the model could be explained, in part, by the stainless steel wire matrix having on average much smaller wire radii than the 50 μm radii assumed in the model, which would necessarily give rise to more retention.

Considerable size variation also existed for both the Fe_2O_3 and magnetite particles. Figure 7 shows particle size distributions obtained with the Accusizer Optical Particle Sizer, Model 770 A and fitted with both bimodal and monomodal log-normal distributions. The corresponding average radii obtained from the monomodal log-normal distributions are presented in Table 1 for both Fe_2O_3 (4.67 μm) and magnetite (2.12 μm). Observe, for example, that the Fe_2O_3 particles had radii of less than a micron up to values of around 40 μm (Fig. 7a) and with two modes instead of one as assumed in the model. Very similar results were obtained with the magnetite particles as shown in Fig. 7b. The magnetite particle radii varied from less than a micron to around 20 μm, and they also exhibited two modes. In the case of the magnetite-silica composite matrix, the over-prediction of the model could be explained, in part, by the marked particle size distribution of the magnetite particles, especially when considering the fact that these particles were composed of clusters of magnetite crystals, as observed in SEMs of the magnetite particles.

SEMs of magnetite particles are shown in Fig. 8. Clearly, the main curvature of a typical magnetite particle, a key element in HGMS, was that

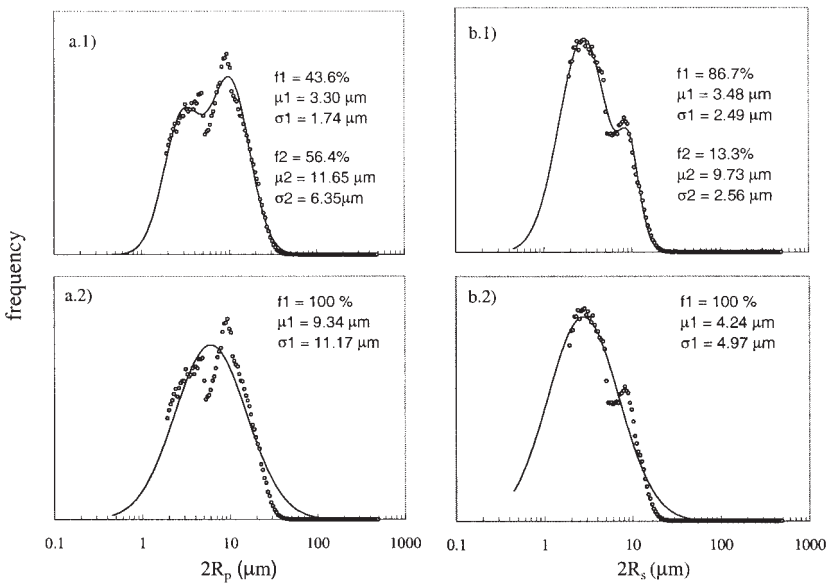

Figure 7. Number particle size distributions of the a) Fe_2O_3 particles, and b) Fe_3O_4 particles obtained from an Accusizer Optical Particle Sizer, Model 770A and fitted to 1) bimodal and 2) monomodal log-normal distributions.

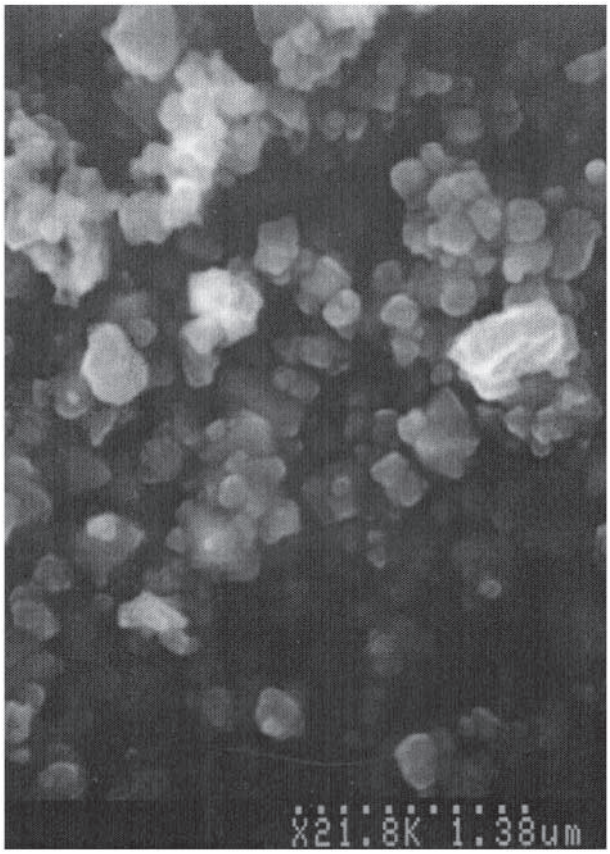

Figure 8. SEM of the pure magnetite particles used to make the 80 wt% magnetite-silica composite matrix element, revealing the 4.24 μm diameter magnetite particles (from Fig. 7) to be comprised of clusters of smaller particles of about 250 nm in diameter.

corresponding to a particle of around 250 nm. In other words, the magnetite particles were composed of large clusters (Fig. 7b) that were further composed of smaller particles of around 250 nm. This result, perhaps, caused magnetite to have magnetic properties associated with not only the larger-sized clusters, but also the far smaller-sized particles within the cluster. Moreover, the high concentration of magnetite in the magnetite-silica composite (i.e., 80 wt%) could have imparted a magnetic attraction contribution from the magnetite-silica composite itself, by behaving as one large magnetic particle but with a saturation magnetization that was equal to that of magnetite corrected by

the volume fraction of magnetite in the magnetite-silica composite. As alluded to earlier, small magnetite particles barely exposed at the surface of the magnetite-silica composite matrix with radii of about 250 nm would not have had the ability to attract and retain the large Fe_2O_3 particles, unless a Fe_2O_3 particle was able to get very close to the surface of such a small magnetite particle,[44] which was doubtful due to their large size and the irregular shape of the composite matrix particle.

Finally, it is interesting to note the intriguing concentration dependence of the ultimate retention observed with the experimental results, something that the models could not predict. These results, perhaps, indicated the existence of dynamic equilibrium at the collection zones, particularly at the external boundaries where the magnetic retention was weaker. When the interactions were very strong, such as those that occurred it the inner regions of the collection zones close to the magnetite particle, it was surmised that monolayers rapidly formed on the magnetite surface essentially independent of the feed concentration. This behavior is akin to that exhibited in the Henry's law region associated with many different kinds of equilibrium phenomena. Extending this argument to higher concentration (multilayer loading) regions beyond the Henry's law region suggested that when the interactions were relatively much weaker, such as those that occurred at the external boundaries of the collection zones far from the magnetite particle, it was surmized that many multilayers formed, not necessarily on the magnetite surface but on the surfaces of the retained Fe_2O_3 particles, and that these multilayers established a dynamic equilibrium that was dependent on the feed concentration. Again, this behavior is akin to that exhibited in the higher-concentration regions beyond the Henry's law region, which is commonly observed with many different kinds of equilibrium phenomena.

CONCLUSIONS

The retention performance of an 80 wt% magnetite-silica composite HGMS matrix element was compared with a stainless steel wool HGMS matrix element. Breakthrough and ultimate (strictly magnetic) retention experiments were carried out at different feed concentrations, flow velocities, and magnetic field intensities with an aqueous slurry containing iron oxide (Fe_2O_3) particles. Results from the ultimate retention experiments were also compared to those obtained from a potential flow model. Overall, magnetite, when adequately supported, proved to be an effective matrix element for use in HGMS systems. The experimental results indicated that magnetite, when supported by silica in the form of an 80 wt% magnetite-silica composite, was about 30 to 40% as effective as stainless steel in retaining iron oxide,

which was quite encouraging when considering that the magnetic saturation of magnetite is about five times smaller than that of stainless steel. The breakthrough profiles obtained with the 80 wt% magnetite-silica composite were also much smoother in appearance than those obtained with the stainless steel wool, possibly indicating that the magnetite-silica composite is a better flow stabilizer than the stainless steel wool. Considering the fact that magnetite is less expensive than stainless steel wool, even when encased in silica gel, makes the use of magnetite as an HGMS matrix element even more attractive for certain applications.

The ultimate retentions predicted from the potential flow model, being of the same order of magnitude as the experimental results, were somewhat surprising yet encouraging. In the case of the stainless steel cylinder, the model under-predicted the experimental results by as much as a factor of 7, whereas in the case of the magnetite spheres, the model over-predicted the experimental results but only by as much as a factor of 3. Several reasons for these discrepancies were discussed and centered on the inherent difficulty of mathematically describing the flow behavior around these kinds of HGMS matrix elements. For example, the overwhelming complexity of the actual retention process caused by the relatively wide size distributions of the Fe_2O_3 particles and both the magnetic matrix elements was not accounted for by the model. Moreover, the potential flow model could not account for the effects of laminar layers and separation zones on retention; nor could it account for the effects of the changing flow patterns caused by particle build-up on retention. Also, the models could not predict the interesting dependence of the ultimate retention on the feed concentration, which was observed experimentally by both matrix elements. This last result suggested that magnetic retention phenomenon could be exhibiting a kind of dynamic equilibrium at the external boundaries of the collection zones where the magnetic force was weaker. Future work will address these issues.

NOMENCLATURE

c_o	Feed concentration of paramagnetic particles, $g\,L^{-1}$
f	Collection efficiency of a ferromagnetic element
F_D	Drag force over a paramagnetic particle, N
F_M	Magnetic force on a paramagnetic particle, N
H_o	Applied magnetic field, $A\,m^{-1}$
k	Demagnetizing factor of a ferromagnetic element
k_b	Boltzmann constant, $J\,K^{-1}$
m	Mass of ferromagnetic material in a matrix, g
M	Magnetization of a ferromagnetic element, $A\,m^{-1}$

M_{sat}	Magnetization of a ferromagnetic element at saturation, $\mathrm{A\,m^{-1}}$
q	Mass loading of paramagnetic material per mass of ferromagnetic element, $\mathrm{g\,g^{-1}}$
r	Distance to the center of a ferromagnetic element, m
R	Radius of a ferromagnetic element, m
R_p	Radius of a paramagnetic particle, m
$R_{m\text{-}s}$	Radius of a magnetite-silica composite particle, m
T	Temperature, K
V_m	Magnetic velocity, $\mathrm{m\,s^{-1}}$
V_o	Velocity of the flow at infinity, $\mathrm{m\,s^{-1}}$
V_p	Volume of a paramagnetic particle, $\mathrm{m^3}$
V_{cp}	Volume of collected paramagnetic particles on one ferromagnetic element.
$\dot{V}$	Volumetric feed flow rate, $\mathrm{cc\,min^{-1}}$

Greek letters

χ_p	Volumetric susceptibility of the particles (SI)
χ_f	Volumetric susceptibility of the medium (SI)
ε_p	Porosity of the collected paramagnetic particles
μ_o	Permeability of free space, $4\pi \times 10^{-7}\,\mathrm{T\,m\,A^{-1}}$
ρ	Density of a ferromagnetic element, $\mathrm{kg\,m^{-3}}$
ρ_p	Density of the suspended particles, $\mathrm{kg\,m^{-3}}$
η_f	Viscosity of the medium, $\mathrm{kg\,m^{-1}\,s^{-1}}$
γ	Angle between the polar angular unitary vectors $\mathbf{e}_\theta$ and $\mathbf{e}_{\theta'}$,
θ	Polar angle
ϕ	Azymuthal angle

Subscripts and Superscripts

c	Ferromagnetic cylinder
s	Ferromagnetic sphere
r	Radial
BT	Breakthrough
ext	External boundary of collection profile
int	Internal boundary of collection profile
sat	Magnetic saturation
θ	Polar angular
ϕ	Azimuthal
$'$	Spherical coordinates according to plane B in Fig. 4b

ACKNOWLEDGMENTS

The authors gratefully acknowledge financial support from the National Science Foundation under grant No. CTS-9985489.

REFERENCES

1. Allen, D.M. *Treatment of Combined Sewer Overflows by High Gradient Separation*; Report 600/2-78-209; US EPA, 1978.
2. Iannicelli, J. New developments in magnetic separation. IEEE Trans. Magn. **1976**, *12*, 436.
3. Kelly, E.G.; Spottiswood, D.J. *Introduction to Mineral Processing*; John Wiley & Sons: New York, 1982.
4. Oder, R.R. High gradient magnetic separation theory and applications. IEEE Trans. Magn. **1976**, *12*, 428.
5. Watson, J.H.P. High gradient magnetic separation. In *Solid–Liquid Separation*, 3rd ed.; Svarovsky, L., Ed.; Butterworth-Heinemann: Oxford, 1990.
6. Norrgran, D.A. Remove unwanted materials with magnetic separators. Chem. Eng. Prog. **1996**, *5*, 56.
7. Avens, L.R.; Gallegos, L.A.; McFarlan, K.J. Magnetic separation as a plutonium residue enrichment processes. Sep. Sci. Technol. **1990**, *25*, 1967.
8. Avens, L.R.; Worl, L.A.; Schake, A.; Padilla, D.D.; Prenger, F.C.; Hill, D.D. *Use of High Gradient Magnetic Separation for Actinide Applications*; US DOE Report LANL LA-UR-96-2064, 1996.
9. Avens, L.R.; Worl, L.A.; de Aguero, K.J.; Prenger, F.C.; Stewart, W.F.; Hill, D.D.; Tolt, T.L. Environmental Remediation using Magnetic Separation, presented at the AIChE Annual Meeting, Miami Beach, FL, November, 1992.
10. Prenger, F.C.; Stewart, W.F.; Hill, D.D.; Avens, L.R.; Schake, A.; de Aguero, K.J.; Padilla, D.D.; Worl, L.A. *High Gradient Magnetic Separation Applied to Environmental Remediation*; US DOE Report LANL LA-UR-93-2516, 1993.
11. Schake, L.R.; Avens, D.D.; Hill, D.D.; Padilla, F.C.; Prenger, D.A.; Romero, T.L.; Tolt Worl, L.A. *Magnetic Separation for Environmental Remediation*; US DOE Report LANL LA-UR-94-3373, 1994.
12. Worl, L.A.; Hill, D.D.; Padilla, D.D.; Prenger, F.C. *High Gradient Magnetic Separation for Nuclear Material Collection*US DOE Report LANL LA-UR-97-1508, 1997.

13. De Latour, C. Magnetic separation in water pollution control. IEEE Trans. Magnetics **1973**, *9*, 314.
14. De Latour, C.; Kolm, H. Magnetic separation in water pollution control. IEEE Trans. Magn. **1975**, *11*, 1570.
15. Mitchell, R.; Bitton, G.; Oberteuffer, J.A. High gradient magnetic filtration of magnetic and non-magnetic contaminants from water. Sep. Purif. Meth. **1975**, *4*, 267.
16. Tsouris, C.; Scott, T.C. Flocculation of paramagnetic particles in a magnetic field. J. Colloid Interf. Sci. **1995**, *171*, 319.
17. Tsouris, C.; Scott, T.C.; Harris, M.T. Para- and dia-magnetic flocculation in a magnetic field. Sep. Sci. Technol. **1995**, *30*, 140.
18. Tsouris, C.; Yiacoumi, S. Particle flocculation and filtration by high-gradient magnetic fields. Sep. Sci. Technol. **1997**, *32*, 599.
19. Tsouris, C.; Yiacoumi, S.; Scott, T.C. Kinetics of heterogeneous magnetic floculation using a bivariate population-balance equation. Chem. Eng. Commun. **1995**, *137*, 147.
20. Yiacumi, S.; Rountree, D.A.; Tsouris, C. Mechanism of particle flocculation by magnetic seeding. J. Colloid Interf. Sci. **1996**, *184*, 477.
21. Home, G.P.; Stockley, M.; Shaw, G. The sirofloc process at redmires water-treatment works. J. IWEM. **1992**, *6*, 10.
22. Kochen, R.L.; Navratil, J.D. Removal of Radioactive Materials and Heavy Metals from Water Using Magnetic Resin. US Patent 5,595,666, 1997a.
23. Kochen, R.L.; Navratil, J.D. Method for Regenerating Magnetic Polyamine Epichlorohydrin Resin. US Patent 5,652,190, 1997b.
24. Ebner, A.D.; Ritter, J.A.; Ploehn, H.J. Magnetic hetero-flocculation of paramagnetic colloidal particles. J. Colloid Interf. Sci. **2000**, *225*, 39.
25. Ebner, A.D.; Ritter, J.A.; Ploehn, H.J.; Kochen, R.L.; Navratil, J.D. New magnetic field-enhanced process for the treatment of aqueous wastes. Sep. Sci. Technol. **1999**, *34*, 1277.
26. Ebner, A.D.; Ritter, J.A.; Ploehn, H.J. Feasibility and limitations of nano-level high gradient magnetic separation. Sep. Purif. Technol. **1997**, *11*, 199.
27. Ebner, A.D. Theoretical and Experimental Developments in Nano and Traditional High Gradient Magnetic Separation; University of South Carolina, 2000; Ph.D. Dissertation.
28. Shen, J.; Ebner, A.D.; Ritter, J.A. Estimation of the points of zero charge and intrinsic equilibrium constants of silica-magnetite composite oxides. J. Colloid Interf. Sci. **1999**, *214*, 333.
29. Ying, T.Y.; Yiacoumi, S.; Tsouris, C. High-gradient magnetically seeded filtration. Chem. Eng. Sci. **2000**, *55*, 1101.
30. Cowen, C.; Friedlaender, F.J. Single wire model of high gradient magnetic separation processes III. IEEE Trans. Magn. **1977**, *13*, 1483.

31. Cowen, C.; Friedlaender, F.J.; Jaluria, R. Single wire model of high gradient magnetic separation processes I. IEEE Trans. Magn. **1976**, *12*, 466.
32. Cummings, D.L.; Himmelblau, D.A.; Oberteuffer, J.A. Capture of small paramagnetic particles by magnetic forces from low speed fluid flows. AIChE J. **1976**, *22*, 569.
33. Friedlaender, F.J.; Gerber, R.; Henkel, H-P.; Birss, R.R. Particle buildup on single spheres in HGMS. IEEE Trans. Magn. **1981**, *17*, 2804.
34. Friedlaender, F.J.; Gerber, R.; Kurz, W.; Birss, R.R. Particle motion near and capture on single spheres in HGMS. IEEE Trans. Magn. **1981**, *17*, 2801.
35. Luborsky, F.E.; Drummond, B.J. Buildup of particles on fibers in a high field-high gradient separator. IEEE Trans. Magn. **1976**, *12*, 463.
36. Luborsky, F.E.; Drummond, B.J. High gradient magnetic separation: theory versus experiment. IEEE Trans. Magn. **1975**, *11*, 1696.
37. Friedlaender, F.J.; Takayasu, M.; Rettig, J.B.; Kentzer, C.P. Studies of single wire parallel stream type HGMS. IEEE Trans. Magn. **1978**, *14*, 404.
38. Takayasu, M.; Gerber, R.; Friedlaender, F.J. Magnetic separation of submicron particles. IEEE Trans. Magn. **1983**, *19*, 2112.
39. Gerber, R.; Krist, P.; Tarrant, L. The retention of strongly magnetic particles in single wire HGMS. IEEE Trans. Magn. **1996**, *32*, 5100.
40. Gerber, R. Magnetic Separation. In *Applied Magnetism*, Gerber, R., Wright, C.D., Asti, G., Eds.; Kluwer Academic Publishers: Dordrecht, NATO ASI Series, Series E: applied Sciences; 1994; Vol. 253, 165.
41. Gerber, R.; Takayasu, M.; Friedlaender, F.J. Generalization of HGMS theory: the capture of ultra-fine particles. IEEE Trans. Magn. **1983**, *19*, 2115.
42. Gerber, R.; Birss, R.R. High Gradient Magnetic Separation. J. Wiley & Sons: Chichester, 1983.
43. Gerber, R. Particle capture in high gradient magnetic separation. In *Physics Programs*, Boardman, A.D., Eds.; J. Wiley & Sons: Chichester, 1980.
44. Ebner, A.D.; Ritter, J.A.; Ploehn, H.J. Magnetic field orientation and spatial effects on the retention of paramagnetic nanoparticles with magnetite. Sep. Sci. Technol. **2002**, *37*, 3727.
45. Ebner, A.D.; Ritter, J.A. Retention of paramagnetic particular by magnetite particle clusters with multifunctional character. Sep. Sci. Technol. **2004**, *39*, 2785–2808.
46. *Handbook of Chemistry and Physics*, 62 Ed.; CRC Press: Section E; 1981–1982.